Effect of material anisotropy on guided wave propagation and scattering in CFRP laminates

F. Hervin, P. Fromme

SPIE.

Effect of material anisotropy on guided wave propagation and scattering in CFRP laminates

F. Hervin and P. Fromme

Department of Mechanical Engineering, University College London, WC1E 7JE, UK

ABSTRACT

Carbon fiber laminates, consisting of highly anisotropic fiber-matrix ply-layers, are widely used in aerospace applications due to their good strength to weight ratio. However, poor interlaminar strength makes them prone to barely visible impact damage (BVID), significantly reducing the load bearing capacity of aircraft components. Guided ultrasonic waves have been widely used for structural health monitoring (SHM) of composite structures. Guided wave propagation and scattering at circular delaminations in a quasi-isotropic laminate was modelled using full three-dimensional (3D) Finite Element (FE) simulations in ABAQUS. Non-contact laser measurements were performed to obtain the scattered wavefield at a film insert delamination. The influence of ply layer anisotropy and incident wave direction were investigated both numerically and experimentally. Scattering directivity patterns were calculated using a baseline subtraction method and 2D scattering matrices were obtained for all incident wave directions. Circular magnets were used as a scattering target and numerical and measured scattering patterns were compared with those of the insert delamination. Strong directional dependency was observed for incident and scattered waves around both delamination and magnets, indicating energy focusing along the outer ply layers of the laminate. For the delamination a strong forward wave was observed, with low amplitude in other directions, whereas the magnet blocked forward transmission of the wave, demonstrating distinct scattering behavior. The anisotropic effects and different scattering patterns should be considered for guided wave sparse array SHM to ensure the robustness of imaging algorithms.

Keywords: Guided Ultrasonic Waves, Finite Element Modelling, BVID, Anisotropy, CFRP, Delamination.

1. INTRODUCTION

Carbon fiber reinforced polymer (CFRP) laminates have good strength to weight ratio and are increasingly being selected for aerospace applications. They consist of a number of highly anisotropic fiber-matrix ply layers, resulting in high in-plane strength, but leaving them vulnerable to damage from low velocity impacts [1]. Barely visible impact damage can develop below the laminate surface, causing significant strength reduction [2]. Robust structural health monitoring (SHM) techniques are required to detect delamination damage in composites in order to prevent catastrophic failure of components.

Ultrasonic guided waves are a promising SHM solution to rapidly interrogate large areas of a composite structure. Low frequencies are desirable to minimize the effects of attenuation in composites and to avoid generation of higher order wave modes [3]. The fundamental symmetric S_0 Lamb mode has been used in several studies to detect delamination damage as it has the fastest propagation velocity and is therefore easy to distinguish experimentally [4]. However, the S_0 mode is not sensitive to delamination damage at interfaces with zero shear strain [5]. In contrast, the fundamental antisymmetric A_0 guided wave mode is sensitive to delaminations at all depths and has a shorter wavelength at the same frequency, resulting in improved sensitivity for smaller defects in composites. Fiber reinforced composites have highly anisotropic material properties, which can impact guided wave propagation. Wave energy is focused towards the high stiffness fiber directions, resulting in higher phase and group velocity in these directions, in addition to wave skewing behavior [6]. Velocity distributions are strongly dependent on the ply layup of the laminate, with the A_0 mode showing less directional dependency compared to the S_0 mode [7]. Focusing of the A_0 mode, however, is still significant enough to impact SHM.

Sparse array imaging, using a network of piezoelectric sensors, provides a cost efficient in-situ SHM solution [8]. Numerous imaging algorithms have been developed to localize damage including delay and sum (DAS) [9], multipath [10], minimum variance (MV) [8] and minimum variance distortionless response (MVDR) imaging [11]. The latter three techniques adaptively weight signals based on known scattering characteristics of a particular defect, which results in improved imaging with fewer artefacts compared to DAS. 2D scattering matrices are often used to summarize scattering

information for a defect [11, 12]. The presence of material anisotropy impacts the performance of sparse array imaging [13]. Whilst some methods are robust for mild anisotropy, severe anisotropy needs to be accounted for in the imaging algorithms. Rather few studies have looked at the influence of anisotropy on guided wave scattering, and subsequently sparse array imaging performance.

Impact damage in composite laminates is often complex and multi-modal, consisting of fiber breakage, matrix cracks, and delaminations [1, 2]. Delamination damage causes the most severe strength reduction and is therefore a critical failure mode. As guided waves enter a delaminated region, waves propagate in each of the sub laminates. Multiple reflections back and forth in the sub-laminates form standing waves, resulting in an increased "trapped" amplitude on top of the delamination [14]. The wave trapping phenomena can be exploited to locate damage, and arrival times of multiple reflections can be used to estimate delamination size [15]. Recombination of the waves propagating in the sub-laminates occur at the delamination exit, resulting in forward and back-scattered waves. The amplitude of the forward scattered wave is dependent on the delamination size, shape, and thickness of the sub-laminate (i.e., delamination depth) [7, 16, 17]. Delaminations located at an asymmetric depth experience high trapped amplitude on top of the delamination, with some forward scattering occurring, whereas delaminations located towards the mid-plane experience a much greater forward scattered amplitude, but limited wave trapping [18, 19]. Anisotropy of individual ply layers, and the layup of the laminate can influence guided wave propagation and scattering directivity [20]. Scattering directivity has been found to be dependent on layup sequence, even for laminates with the same number of ply layers [7]. Fiber steering effects of the S_0 mode result in energy focusing along the laminate fiber directions, with higher incident and scattered amplitudes observed [21].

Specimens containing artificial delaminations, created by placing a film between the ply layers during manufacturing, are often used to study guided wave scattering in composites. This allows for the size, location, and depth of damage to be controlled. To avoid the requirement for multiple specimens with permanent damage for the development and testing of SHM algorithms, magnets, placed on opposite sides of a structure, are easily removed from a specimen and have been used in several studies to simulate damage [11, 22]. Scattering directivity around a magnet has, however, not been studied numerically for composites.

In this work full scattering characteristics of the A_0 guided wave mode a delamination and magnet target are obtained through Finite Element (FE) simulation for a quasi-isotropic CFRP panel. The influence of incident wave propagation direction, and therefore material anisotropy, on scattering is investigated. Non-contact laser measurements are performed around an artificial insert delamination at asymmetric depth, and magnets mounted on an undamaged region of the composite plate respectively, to validate the FE results. 2D scattering matrices were calculated from FE baseline subtraction data for a circular asymmetric depth delamination, midplane depth delamination, and permanent magnet. Implications of anisotropy on guided wave sparse array SHM are discussed.

2. EXPERIMENTAL MEASUREMENTS

Non-contact laser measurements were performed on an 8-ply quasi-isotropic CFRP panel with ply stacking sequence [-45/45/90/0]$_s$. The specimen with dimensions 600mmx600mmx1.6mm was manufactured from unidirectional pre-preg plies with nominal thickness 0.2mm and material properties as presented in Table 1. During manufacturing a circular film insert (diameter 15mm, thickness 0.2mm) was placed at the center of the plate between the second and third plies (depth 0.4mm) to produce an artificial delamination. An ultrasonic C-scan was performed to verify the presence and shape of the delaminations, which had nominal dimensions of 20mmx16mm [23]. Circular neodymium magnets (NdFeB, diameter 20mm) were mounted on both sides of an undamaged region of the plate and used as scattering targets, as shown schematically in Fig. 1a. Set honey was used to couple the magnets to the plate surface.

Piezoelectric transducers were bonded to the plate surface using cyanoacrylate glue. Transducers were glued 100mm from the delamination and magnet center in the 0°, 45°, -45°, and 90° directions to investigate scattering for different incident wave directions (Fig. 1a/b). A single transducer was excited with a 50kHz (center frequency) 5 cycle sine wave modulated by a Hanning window using a programmable function generator, The excitation signal was amplified to 25Vpp before being applied to the transducer. A laser vibrometer, attached to a scanning rig, was used to measure the velocity of the out-of-plane displacement at the plate surface. Retroreflective tape was applied to the plate surface to improve laser beam reflection and subsequently the signal to noise ratio. Tape was removed underneath the magnet to improve coupling (Fig. 1b inset). Time signals were filtered using a band-pass filter with cut-off frequencies of 25kHz and 75kHz respectively. A digital storage oscilloscope was used to average signals 20 times before being saved to a PC for further analysis in MATLAB. A circle of measurement points, 30mm radius, centered on the delamination and magnet respectively was scanned in 2° increments. Measurements were repeated for each incident wave propagation direction.
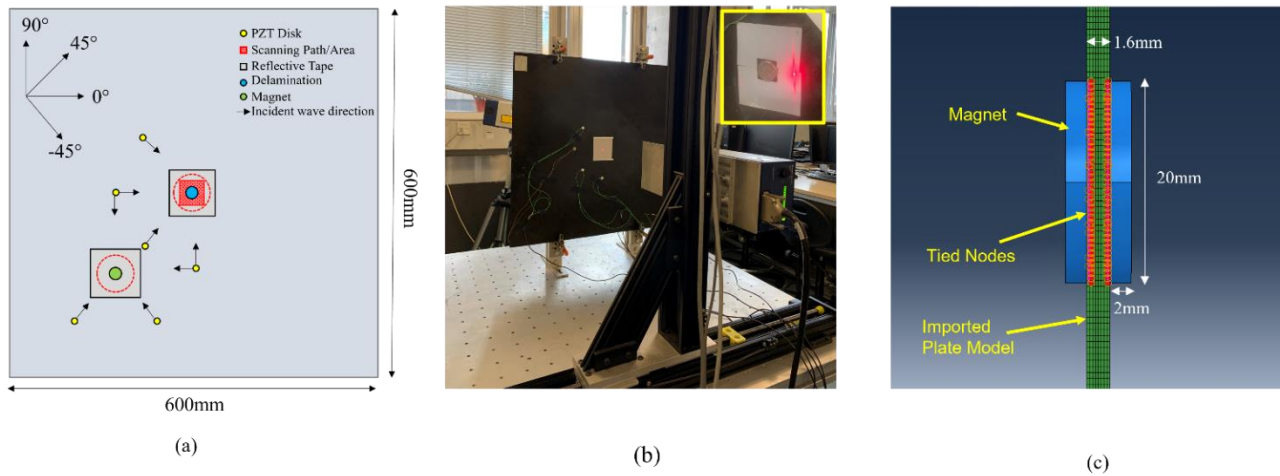
Figure 1: (a) Schematic of damage, transducer and scanning locations on composite plate; (b) Photograph of experimental setup and mounted magnets (inset); (c) ABAQUS screenshot of FE magnet model with tied nodes highlighted.

Table 1: Engineering constants for a single ply layer of the CFRP laminate. Moduli are given in GPa [23].

E_1	E_2	E_3	G_{12}	G_{13}	G_{23}	ν_{12}	ν_{13}	ν_{23}	ρ [kg/m^3]
175	6.90	6.90	4.18	4.18	2.35	0.25	0.25	0.46	1520

Table 2: Material properties for magnets (NdFeB).

Material Property	Value
E	160 GPa
ν	0.24
ρ	7500 kg/m^3

3. FINITE ELEMENT SIMULATIONS

Full 3D FE simulations of the CFRP panel, with the same dimensions as the physical specimen, were performed in ABAQUS/Explicit. A model input file specifying model parameters and geometry was generated in MATLAB before being imported into ABAQUS for analysis. Eight node solid brick elements (C3D8R) were selected for the model with each ply layer modeled as a single layer of elements with unidirectional material properties given in Table 1. The orientation of the material properties of each layer was rotated to match the stacking sequence of the specimen. A uniform mesh with element size of 0.5mmx0.5mmx0.2mm and time increment of 50ns was selected to produce stable simulations. Rayleigh damping was incorporated into the model to simulate wave attenuation. The stiffness proportional damping coefficient was set to β=30ns for all simulations. Excitation of the A_0 mode was modelled by applying an out-of-plane force to a single node with a 50kHz 5 cycle sine wave with Hanning window to match the experiments. The position of the excitation node was varied to model different incident wave directions but kept at a distance of 100mm from the center of the plate. Incident wave directions between -90° and +90° degrees were modelled in 5° increments. History outputs of the out-of-plane displacements were recorded for a 60mm grid of measurement points (1mm step size) at the center of the plate for all simulation cases. From this a 30mm circle of points can be selected and interpolated during analysis to match the experiments.

A 20mm diameter circular zero volume delamination was incorporated into the model by overwriting existing elements at the delamination location [19]. A square area of new nodes with approximate dimensions of the delamination, connected

to one side of the plate, were defined. A node-to-node tie constraint was then applied to form the edges of the circular delamination. A bilinear interpolation was used to map the circle onto the Cartesian grid. The delamination was initially placed at the center of the plate between the second and third plies (0.4mm) depth to match the experiments. A delamination at the midplane of the plate (0.8mm depth) was also modelled. Baseline simulations containing no damage were produced for each incident wave direction. In order to model scattering around a permanent magnet the baseline model was modified to include an additional set of nodes in a circular region (diameter 20mm) on the front and rear of the plate. The model was then imported into ABAQUS CAE to model magnets mounted on the plate. Two cylindrical parts (diameter 20mm, thickness 2mm) were defined and tied to the circular node sets on the plate using a node-to-surface tie constraint as shown in Fig. 1c [24]. Material properties of NeFeB were assigned to the magnet parts as given in Table 2.

4. SCATTERING AROUND DELAMINATION AND MAGNET TARGETS

The displacement magnitude contour plots in Fig. 2 were obtained from the FE model at 165ns for both the delamination (ply 23, Fig. 2a) and magnet (Fig. 2b) targets. The contours are shown for the 0° incident wave direction. For both cases the incident wavefront is not circular due to the anisotropy of the laminate, resulting in higher amplitude in the diagonal directions (+/-45°), in addition to slightly higher wave velocities. These directions correspond to the fiber orientation of the outer ply layers of the laminate, indicating that energy focusing is occurring along the outer plies. The delamination and magnet cases show distinct scattering behavior. For the delamination a forward scattered lobe can be observed with two shadow regions of destructive interference either side. Limited backscattering is observed. On the other hand, the permanent magnet blocks propagation of the wave pulse, resulting in a large back-scattered wave amplitude. Interference between incident and sideways scattered waves can also be observed.
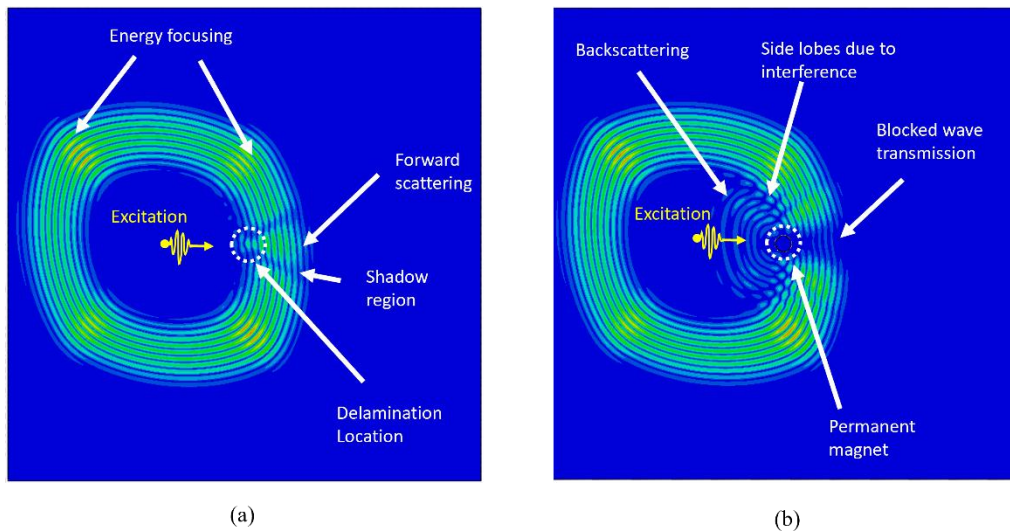

Figure 2: Displacement magnitude contour plots for scattering around a) ply 23 delamination b) magnet target.

The wave amplitude around a 30mm circle of measurement points was obtained for both delamination and magnet cases by calculating the magnitude of the FFT at the center frequency (50kHz) for each time trace. The experimental and simulated scattering patterns scattering patterns for the 0° and 45° incident wave directions are shown in Fig. 3 for the delamination (Fig. 3a/b) and magnet (Fig. 3c/d) cases. Overall good agreement between experiment and simulation is observed. For the delamination a strong forward scattered lobe can be observed for both the 0° and 45° directions, although the lobe is less distinct in the FE simulations. Compared to the 0° direction, the +45° scattering pattern is elongated and slightly asymmetric. Forward and backscattered amplitudes are higher in the +45° direction, which again indicates energy focusing is occurring towards the outer ply layers. These results indicate that scattering around a circular delamination is strongly directionally dependent due to the material anisotropy.

For the permanent magnet, no forward scattered lobe is present in either direction, indicating blocking of the incident wave as expected from the contour plot in Fig. 2b. The FE scattering patterns in Fig. 3c/d are symmetric with additional lobes, perpendicular to the respective incident wave direction. The scattering around the magnet is distinctly different to that of

the delamination case. The magnet scattering again shows directional dependency and a higher backscattered amplitude is observed for the +45° direction, indicating energy focusing towards this direction. Excellent agreement between the magnet FE and experiment can be observed for the +45° direction. For the 0° direction the overall number and position of lobes are similar, although there is some variation in amplitude. The experimental measurements used honey to couple the magnet to the plate, whereas the FE model used an idealized tied contact condition, and nominal material properties which could be causing the discrepancies. Overall, the FE magnet model shows good agreement with the experiments and captures the key scattering behavior of blocking forward transmission.
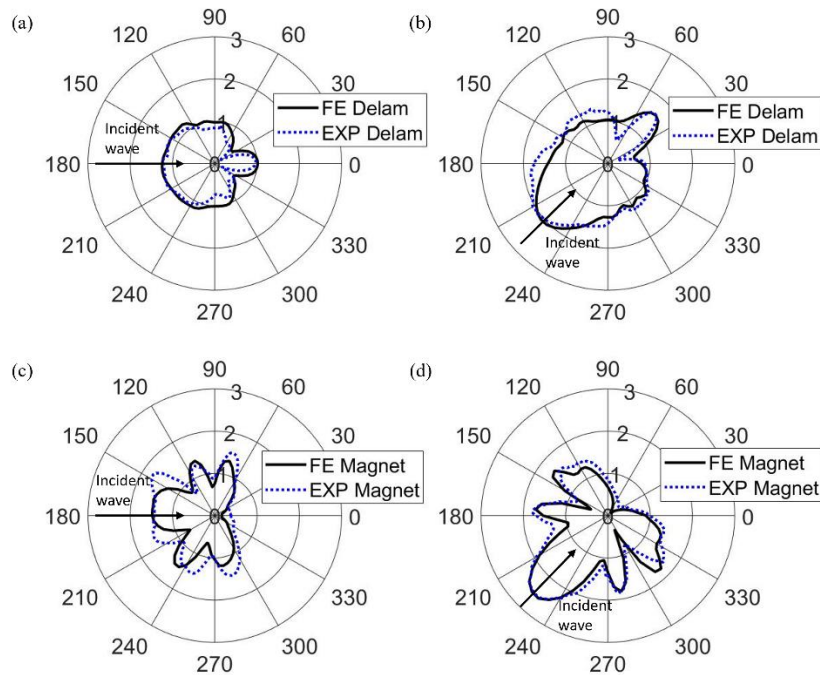

Figure 3: Measured and simulated FFT magnitude around a 30mm circle of measurement points for ply 23 delamination in a) 0° b) +45° and magnet in c) 0° d) +45° incident wave directions.

5.   SCATTERING MATRICES

The FE model for both the delamination and magnet were validated against experiments, as shown above. The amplitude patterns in Fig. 3 include both the incident and scattered components of the wave. A baseline subtraction analysis was performed on the FE results in order to isolate the scattered wave. The complex difference of the FFT magnitude of the damage and baseline simulation was calculated, as this preserves both amplitude and phase information. The polar plots of the isolated scattered wave are shown for the 0° and +45° directions for the ply 23 delamination (Fig. 4 a/b), midplane delamination (Fig. 5a/b) and magnet (Fig. 6a/b), respectively. Scattering matrices allow for the visualization of the full scattering characteristics of a defect and display the baseline subtraction data for all direction. For each of the three damage types, the isolated scattered wave was calculated for simulations with incident wave directions between -90° and +90° in 5° increments. As the simulated damage cases presented here are symmetric, the scattering is reversible. Scattering data for the remaining angles could be therefore obtained from existing cases rotated by 180°. The 2D scattering matrices shown in Fig. 4c/5c/6c were plotted for each incident direction θ_i against respective scattered directions θ_s (5° increments). Each column of the matrix corresponds to the amplitudes of a single polar plot.

The baseline subtraction plots, and 2D scattering matrix for the ply 23 delamination are shown in Fig. 4. For each of the incident wave directions there is a large forward scattered lobe with only very small back-scattered amplitude, in addition to significant reduction in the sideways scattered amplitude. A significant increase in forward scattered amplitude can be seen in the 45° direction (Fig. 4b) compared to the 0° direction (Fig. 4a). These results, in addition to those presented in

Fig. 3a/b indicate that the incident wave direction has a significant influence on the scattering around a circular delamination, due to the anisotropic layup of the composite laminate. The scattering matrix for the ply 23 delamination is shown in Fig. 4c (20dB scale). The scattering is dominated by a strong forward scattered wave in all incident wave directions (high amplitude diagonal band). The forward scattered amplitude increases around the +/-45° and +/-135° incident wave directions, which further indicates that energy focusing is occurring along the fiber directions of the outer ply layers. There is approximately a 10dB drop in amplitude between forward and backscattered amplitudes either side of the diagonal band. Regions of low scattered amplitude are observed in most directions, which could lead to delaminations being missed depending on their location in relation to a distributed sensor network.
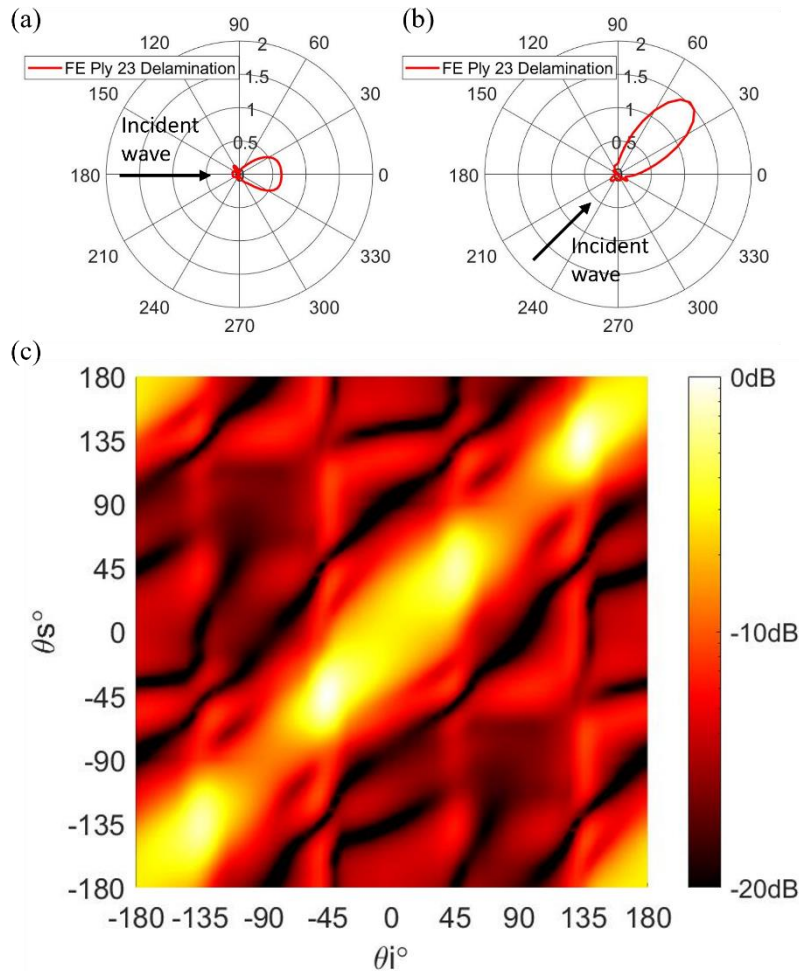

Figure 4: Simulated isolated scattered wave (baseline subtraction) for the ply 23 delamination in the a) 0° b) 45° incident wave directions; c) 2D scattering matrix for ply 23 delamination.

The scattering results for the midplane delamination are presented in Fig. 5. Again, the scattering is dominated by a strong forward scattered wave, with low backscattered amplitude as seen in the polar plots (Fig. 5a/b), and from the diagonal band in the scattering matrix (Fig. 5c, 20dB scale). Whilst the shape of lobes are similar for both delamination depth, the scattered amplitudes for the midplane delamination are significantly higher than those of the ply 23 delamination. The forward scattered amplitude again increases towards the diagonal directions, with regions of low amplitude observed for most incident directions, potentially leading to delaminations being missed. Overall, the scattering matrices show a similar scattering behavior for the different delamination depths.
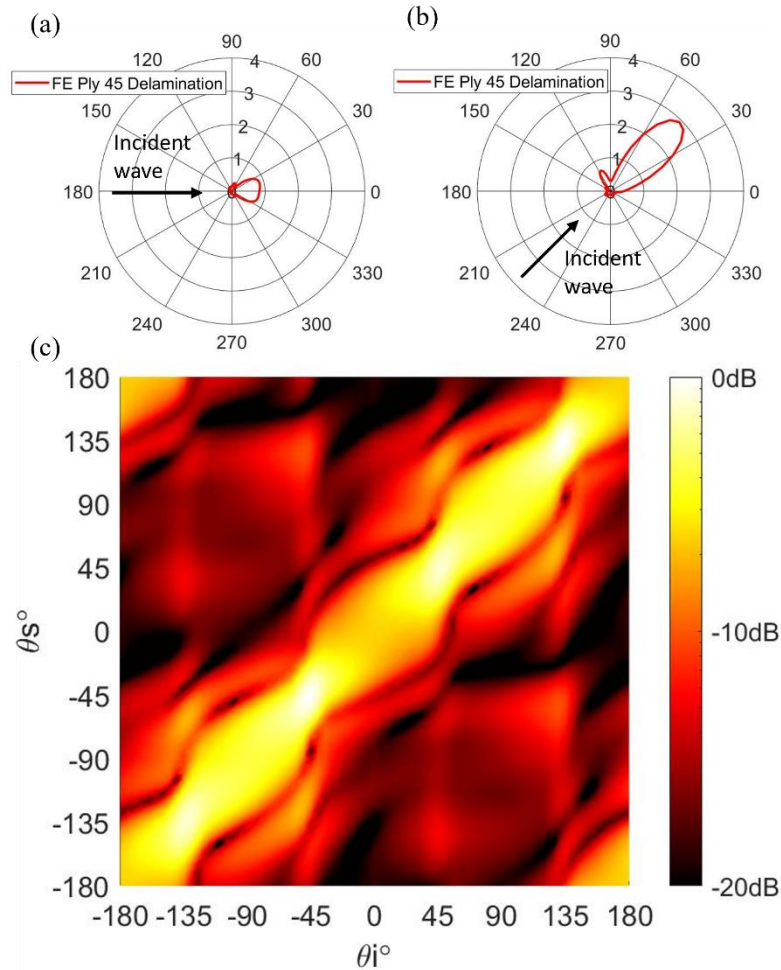
Figure 5: Simulated isolated scattered wave (baseline subtraction) for the ply 45 (midplane) delamination in the a) 0° b) 45° incident wave directions; c) 2D scattering matrix for ply 45 (midplane) delamination.

The scattering results for the magnet model are shown in Fig. 6. Here, the forward scattered wave represents blocking of wave transmission caused by the magnet, which is out of phase with the incident wave. Backscattered amplitudes are significantly higher than observed for the delamination cases, consistent with the amplitudes observed in Fig. 3. Figure 6a shows the scattering directivity pattern for the 0° direction. Scattered amplitude is present in all directions with slightly higher forward and backscattered amplitudes. For the +45° incident wave direction (Fig. 6b) more distinct lobes are present, producing a cross-like pattern. The additional lobes are approximately perpendicular to the incident wave direction (i.e., in the -45° direction), which corresponds to the fiber orientations of the two outermost plies. Energy focusing is again occurring along the diagonal directions. The amplitude in the forward direction is approximately twice that of the backscattered direction. The scattering matrix for the magnet is shown in Fig. 6c (10dB scale) and shows a significantly different scattering pattern compared to the delamination cases above. Again, a diagonal band with higher forward scattered amplitude is observed, but as seen in the polar plots this, slightly counterintuitively, is the result of a drop in amplitude, caused by blocking of wave transmission by the magnet. Additional spots of higher amplitude can be observed for incident wave directions +/-45° +/-135° due to the cross shaped scattering patterns, shown in Fig. 6b, that occur in these directions. Again, energy focusing towards the +/-45° and +/-135° directions is observed. Although lower amplitude is observed in some directions, overall, for the magnets, the ratio of forward to backscattered amplitudes is lower than for the delamination. This is due to scattered amplitude observed in multiple directions in the magnet cases, whereas the delamination cases were dominated by a distinct forward scattered lobe. These results indicate that scattering around a magnet is directionally dependent due to anisotropy of the laminate. However, the magnet displays significantly different scattering behavior compared to a delamination of a similar size.
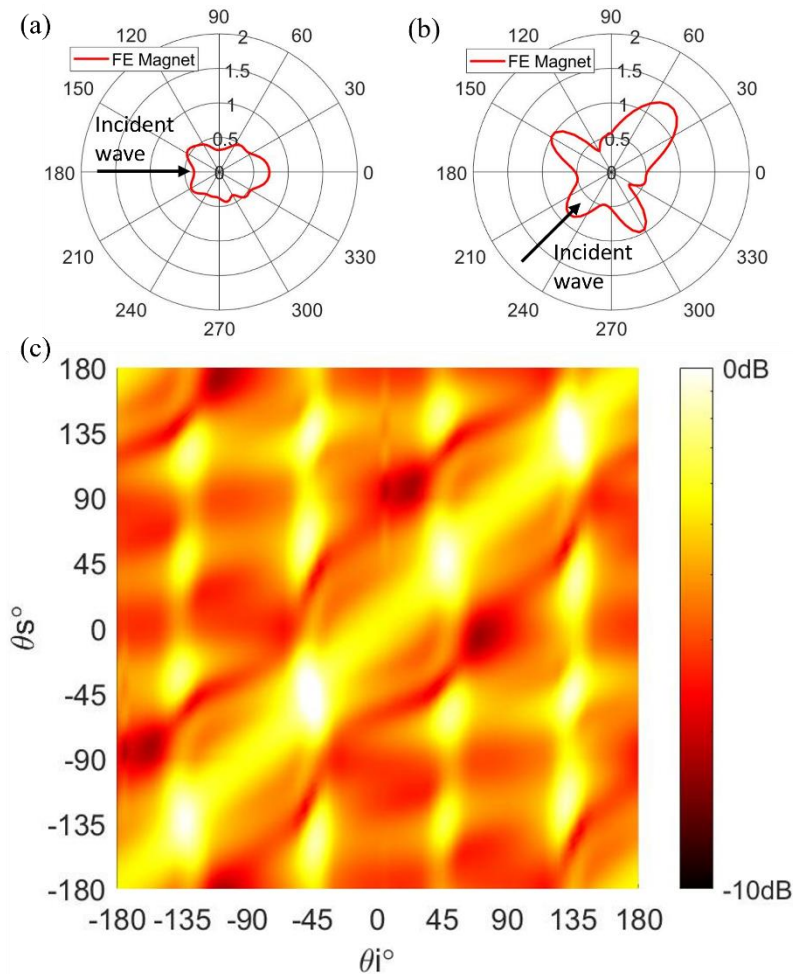
Figure 6: Simulated isolated scattered wave (baseline subtraction) around a magnet in the a) 0° b) 45° incident wave directions; c) 2D scattering matrix for magnet.

6. CONCLUSIONS

The influence of anisotropy on A_0 mode scattering in a quasi-isotropic CFRP laminate was investigated through experiments and FE simulation. Scattering around circular delaminations of different depths and permanent magnets of equivalent size to the delaminations was studied for multiple incident wave directions. Increased amplitude of incident and scattered waves was observed in the fiber orientations of the outer ply layers, due to energy focusing in these directions. Distinct scattering behavior was observed for the delamination and magnet cases, with significant directional dependency for each damage type. Scattering around a delamination was characterized by a strong forward scattered lobe with low scattered amplitude otherwise. The results indicate that guided wave scattering around a delamination in composite structures can be strongly influenced by incident wave direction due to the anisotropy of the laminate. Therefore, imaging algorithms should take the anisotropic effects into account. Scattering patterns around magnets were demonstrated to vary with incident wave propagation direction, although scattered amplitudes were more uniform for different incident wave directions. On the other hand, both the ply 23 and midplane delamination displayed limited scattering except for a strong lobe in the forward direction, which could lead to damage being missed, particularly if the damage is located outside of the area covered by the distributed sensor array. This could indicate that magnets simulating damage are easier to detect with sparse array imaging and that realistic damage types might be missed if imaging algorithms are only tested on magnet targets. Therefore, the robustness of imaging algorithms for the detection of realistic damage should be ascertained.

REFERENCES

[1] Shyr, T.W. and Pan, Y.H., "Impact resistance and damage characteristics of composite laminates," Compos Struct 62, 193–203 (2003).

[2] Cantwell, W. and Morton, J., "Detection of impact damage in CFRP Laminates," Compos Struct 3, 241-257 (1985).

[3] Diamanti, K., Hodgkinson, J.M. and Soutis, C., "Detection of low velocity impact damage in composite plates using Lamb waves," Struct Heal Monit 3, 22-41 (2004).

[4] Hayat, K. and Ha, S.K., "Low-velocity impact-induced delamination detection by use of the S0 guided wave mode in cross-ply composite plates, A numerical study," J Mech Sci Technol 28, 445–455 (2014).

[5] Guo, N. and Cawley, P., "The interaction of Lamb waves with delaminations in composite laminates," J Acoust Soc Am 94, 2240–2246 (1993).

[6] Neau, G., Lowe, M. and Deschamps, M., "Propagation of Lamb waves in anisotropic and absorbing plates, Theoretical derivation and experiments," AIP Conf Proc 615, 1062-1069 (2002).

[7] Veidt, M. and Ng, C.T., "Influence of stacking sequence on scattering characteristics of the fundamental anti-symmetric Lamb wave at through holes in composite laminates," J Acoust Soc Am 129, 1280–1287 (2011).

[8] Hall, J.S., Fromme, P. and Michaels, J.E., "Guided wave damage characterization via minimum variance imaging with a distributed array of ultrasonic sensors," J Nondestruct Eval 33, 299–308 (2014).

[9] Wang, C.H., Rose, J.T. and Chang, F.K., "A synthetic time-reversal imaging method for structural health monitoring," Smart Mate Struct 13, 415-423 (2004).

[10] Hall, J.S. and Michaels, J.E., "Multipath ultrasonic guided wave imaging in complex structures", Struct Heal Monit 13, 345-358 (2015).

[11] Williams, W.B., Michaels, T.E. and Michaels, J.E., "Estimation and application of 2-D scattering matrices for sparse array imaging of simulated damage in composite panels," AIP Conf Proc 1806, 020014 (2017).

[12] Zhang, J., Drinkwater, B. and Wilcox, P., "The use of ultrasonic arrays to characterize crack-like defects," J Nondestr Eval 29, 222-232 (2010).

[13] Ostiguy, P.C., Quaegebeur, N. and Masson, P., "Comparison of model-based damage imaging techniques for transversely isotropic composites," Struct Heal Monit 16, 428-443 (2017).

[14] Hayashi, T. and Kawashima, K., "Multiple reflections of Lamb waves at a delamination," Ultrasonics 40, 193–197, (2002).

[15] Kudela, K., Wandowski, T., Malinowski, P., et al., "Application of scanning laser Doppler vibrometry for delamination detection in composite structures," Op Lasers Eng 99, 46–57 (2017).

[16] Murat, B., Khalili, P. and Fromme, P., "Scattering of guided waves at delaminations in composite plates," J Acoust Soc Am 139, 3044–3052 (2016).

[17] Pudipeddi, G.T., Ng, C. and Kotousov, A., "Mode Conversion and Scattering of Lamb Waves at Delaminations in Composite Laminates," J Aerosp Eng 32, 04019067 (2019).

[18] Ramadas, C., Balasubramaniam, K., Joshi, M., et al., "Interaction of guided Lamb waves with an asymmetrically located delamination in a laminated composite plate," Smart Mate Struct 19, 065009 (2010).

[19] Hervin, F., Maio, L. and Fromme, P., "Guided wave scattering at a delamination in a quasi-isotropic composite laminate: Experiment and simulation," Compos Struct 275, 114406 (2021).

[20] Gupta, S. and Rajagopal, P., "Effect of ply orientation and through-thickness position of delamination on the reflection of fundamental symmetric S0 Lamb mode in GFRP composite plate structures," Ultrasonics 90, 109–119 (2018).

[21] Chiu, W.K., Rose, L.R.F. and Nadarajah, N., "Scattering of the fundamental anti-symmetric Lamb wave by a mid-plane edge delamination in a fiber-composite laminate," Proc Eng 188, 317-324 (2017).

[22] Ebrahimkhanlou, A., Dubuc, B. and Salamone, S., "Damage localization in metallic plate structures using edge reflected Lamb waves," Smart Mate Struct 25, 085035 (2016).

[23] Maio, L., Ricci, F., Memmolo, V., et al., "Application of laser Doppler vibrometry for ultrasonic velocity assessment in a composite panel with defect," Compos. Struct 184, 1030–1039 (2018).

[24] Hervin, F. and Fromme, P., "Anisotropy influence on guided wave scattering for composite structure monitoring," (Manuscript, Submitted Jan 2022)